ACS APPLIED MATERIALS & INTERFACES

www.acsami.org

Research Article

Three-Dimensional Hollow Reduced Graphene Oxide Tube Assembly for Highly Thermally Conductive Phase Change Composites and Efficient Solar−Thermal Energy Conversion

Mingxin Li, Xuanjie Wang, Lilian Odom, Keith Bryce, Dong Zhao, Junhua Shen, Zongwei Ma, Chulsung Bae, Shankar Narayan, and Jie Lian*

Cite This: *ACS Appl. Mater. Interfaces* 2023, 15, 18940−18950

Read Online

ACCESS | Metrics & More | Article Recommendations | Supporting Information

ABSTRACT: Due to their extraordinary mechanical strength and electrical and thermal conductivities, graphene fibers and their derivatives have been widely utilized in various functional applications. In this work, we report the synthesis of a three-dimensional (3D) hollow reduced graphene oxide tube assembly (HrGOTA) using the same wet spinning method as graphene fibers. The HrGOTA has high thermal conductivity and displays the unique capability of encapsulating phase change materials for effective solar−thermal energy conversion. The HrGOTA comprises layers of moisture-fused hollow reduced graphene oxide tubes (HrGOTs), whose individual thermal conductivity is up to 578 W m^{-1} K^{-1}. By impregnating 1-octadecanol into HrGOTs, a 1-octadecanol-filled HrGOT phase change composite (PCC) with a latent heat of 262.5 J g^{-1} is obtained. This high latent heat results from the interfacial interaction between 1-octadecanol and the reduced graphene oxide tube, as evidenced by the shifts in XRD patterns of 1-octadecanol-filled and 1-octadecanol/multiwalled carbon nanotube-filled HrGOTA samples. In addition, 1 wt % multiwalled carbon nanotubes are added to the PCC to enhance visible light absorption. Because of their high thermal conductivity and visible light absorption rates, these new PCCs display high solar−thermal energy conversion and storage efficiencies of up to 81.7%, commensurate with state-of-the-art carbon-based PCCs but with significantly lower carbon weight percentages.

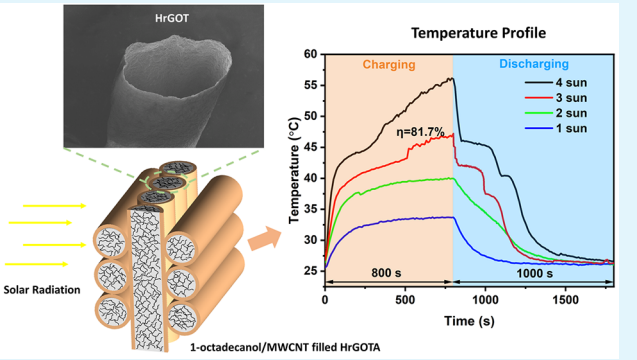

KEYWORDS: *hollow reduced graphene oxide tubes, 1-octadecanol, multiwalled carbon nanotubes, thermal conductivity, solar−thermal energy conversion and storage*

1. INTRODUCTION

Graphene fibers (GFs) are 1D graphene macrostructures that exhibit extraordinary mechanical strength and electrical and thermal conductivities.[1−3] Owing to their thermal conductivities of up to 1500 W m^{-1} K^{-1},[2] GFs have seen great success in Joule heating,[4] thermal regulating graphene fabrics,[5] and thermomechanical actuators.[6,7] Furthermore, as a 3D derivative of GFs, hollow graphene-based tubes have similarly favorable high thermal conductivity while possessing the capacity to encapsulate and interact with other thermally functional materials.[8] This opens up new opportunities for applications in functional materials. One potential application of hollow graphene-based tube assemblies is to encapsulate phase change materials (PCMs), enabling effective thermal transport and mechanical stability/structural integrity for highly efficient thermal storage and solar−thermal energy conversion.

PCMs are thermally functional materials that exchange thermal energy with their surroundings during solid-to-liquid and liquid-to-solid phase change transformations at a constant temperature.[9] Among different categories of PCMs, organic PCMs are the most abundant and inexpensive. Alkanes, fatty alcohols, and fatty acids are the most common categories of organic PCMs and have some common favorable attributes, including high phase change enthalpies, no phase separation during phase change, moderate phase change temperatures, good chemical stability, and biocompatibility.[10] With these advantages, organic PCMs have been widely used in many thermal management and energy storage applications. These applications include thermal insulation in building materials, thermal management of compact electronics, and solar−

Received: January 12, 2023
Accepted: March 30, 2023
Published: April 10, 2023

thermal energy conversion and storage.[11] Nevertheless, some inherent properties of organic PCMs have substantially limited their broader utilization in more advanced functional applications. These inherent drawbacks include leakage in the liquid phase, low absorptance of solar radiation, and limited thermal conductivity.[12−14]

The low thermal conductivity of pristine organic PCMs (<0.5 W m^{-1} K^{-1}) is particularly problematic.[15,16] In practice, heat cannot penetrate through bulk PCM, causing unwanted melting at the outer surfaces. In addition, very low charging and discharging efficiencies also hinder their practical applications.[17] To resolve this issue, a wide range of thermally conductive additives have been incorporated into organic PCMs to form organic PCCs.[18−22] Organic PCCs composited with carbon-based additives generally have high thermal conductivity, low density, low thermal expansion, and outstanding chemical and thermal stability.[23] Being lightweight with extremely high thermal conductivities of up to 5000 W K^{-1} m^{-1}, graphene-based materials have been of particular interest in the use of organic PCCs.[24] Interestingly, those graphene-containing composites have more than 10 times higher thermal conductivity than pristine organic PCMs.[10] This improvement is particularly evident when graphene flakes or interwoven GFs are connected to form a continuous heat transfer pathway in the PCCs.[15,25] Moreover, only small weight percentages of graphene additives are needed to make these improvements possible. In addition to enhancing thermal transport in PCCs, graphene-based materials also have high absorption rates of visible light and can significantly increase the amount of light utilization due to a decrease in reflection compared to pristine PCMs.[26]

The overall performance of solar−thermal energy conversion and storage of organic PCCs greatly benefits from the synergetic effect of graphene-based material's high thermal conductivity and high visible light absorption rates.[27−29] In recent studies, solar−thermal conversion and storage efficiencies have reached an astonishing ∼94% in PCCs with high graphene weight percentages (>10 wt %).[30,31] However, the excess use of graphene results in a significant reduction in the phase change enthalpies and therefore much lower total energy storage capacity in the PCCs than pristine PCMs. Moreover, improvements could also be made to further enhance properties other than solar−thermal conversion and storage efficiencies, such as the PCCs' thermal conductivity, structural integrity, solar absorption capacity, etc. In recent literature, aligned networks of graphene flakes suffer from relatively high interfacial thermal resistivity between individual graphene flakes.[32] In contrast, the PCCs with interconnecting GFs allow for higher thermal conductivity but at the expense of structural integrity due to leakage.[33]

Building upon existing literature on hollow graphene oxide tube (HGOT) fabrication and combining the steps of coaxial wet spinning, chemical reduction, and thermal annealing,[8,34] we develop a novel method for the highly efficient fabrication of HrGOT whose diameters could be parametrically controlled. A PCC is formed by vacuum-impregnating 1-octadecanol, a versatile PCM with high phase change enthalpies, into HrGOTs. Lattice contraction of 1-octadecanol at the interface of graphene and 1-octadecanol results in significantly higher phase change enthalpies of the 1-octadecanol-filled HrGOT PCC than other types of PCCs with similar carbon loading ratios. By adding a moisture-fusing process between the coaxial wet spinning and chemical reduction procedures, HrGOT can be assembled in a layer-by-layer fashion into interconnected 3D macrostructures, which can be further treated to form HrGOTAs. A mixture of 1-octadecanol and multiwalled carbon nanotubes (MWCNTs) was vacuum impregnated into the HrGOTA to form the final 1-octadecanol/MWCNTs-filled HrGOTA PCC applicable for solar−thermal energy conversion and storage. The interconnected HrGOT network is favorable for fully utilizing the entire volume of the PCC for thermal energy storage. It allows rapid 3D thermal transport and provides a framework for ensuring the stability of the PCC by containing 1-octadecanol using surface tension.[35] Additionally, the 1 wt % MWCNTs in the 1-octadecanol-filled HrGOTA PCC further enhances the PCC's visible light absorption. The PCC presented in this work exhibits an excellent solar−thermal conversion and storage efficiency of 81.7% while having 20.4 to 66.7% less carbon than other carbon-based PCCs with similar solar−thermal conversion and storage efficiencies.[20,36] Furthermore, our work demonstrates the high applicational potentials of HrGOTA, which can serve as a versatile interconnected framework for compositing various functional materials with high thermal conductivity and structural integrity at elevated temperatures.

2. EXPERIMENTAL SECTION

2.1. Materials. Graphite intercalation compounds (99.99%, 50 mesh) were purchased from Qingdao Nanshu Graphite Co. Ltd. 1-Octadecanol (97%) and hydroiodic acid (>47%) were purchased from Alfa Aesar. MWCNTs were purchased from Cheap Tubes Inc. Acetone was purchased from Acros Organic. Ethanol (99.5%) was purchased from Sigma-Aldrich. Sulfuric acid (98%), nitric acid (67−69%), ethyl acetate, *n*-hexanes, and *N*,*N*-dimethylformamide (DMF) (99.8%) were purchased from Fisher Chemicals.

2.2. Fabrication of HrGOTs and HrGOTAs. GO was prepared from graphite intercalation compounds using a modified Hummer's method.[37,38] The GO aqueous solution was replaced by DMF using a Sorvall RC-5C plus centrifuge at 13000 rpm for 5 times to reach a concentration of 8 mg mL^{-1}. The GO gel was wet spun through the outer layer of a coaxial needle (with an inner gauge of 22 and an outer gauge of 16) into a coagulation bath composed of an ethyl acetate and acetone mixture. The volumetric ratio of ethyl acetate and acetone is 3:1.[39] A solution with the same composition as the coagulation bath was injected through the inner core of the coaxial needle at 7 mm s^{-1} into the coagulation bath, while the GO dispersion was injected through the outer layer at the same velocity. After 3 min of coagulation, the wet-spun hollow graphene oxide gel tubes can be snipped into shorter segments and washed in *n*-hexanes for 5 s. The tubes were vertically oriented on a ceramic block and then cut open at the ends with a sharp razor so that the fluid within the bore of the tubes drained out. The drained tubes were dried on the ceramic block for a limited amount of time before the ends of the tubes were pinched shut. The tubes were fully dried by suspending them across the top of a ceramic crucible at their ends, forming precursor HGOTs. Minimum space was left between these tubes by placing them closely parallel to one another. The entire top of the crucible was covered by the tubes forming the first layer of an HGOT assembly, which was then dried for at least 10 min. When all the tubes on the first layer were dried, the bore coagulation liquid was drained from another freshly wet-spun gel tube layer of appropriate length. Using flat-tipped tweezers, the two ends of this gel tube were pinch-sealed. The outer surface of this pinched tube was then wetted by submersion in a mixture of ethanol and water (volume ratio of 1:3) for 1 s.[4] The wetted tubes were closely laid next to each other perpendicularly on top of the first layer of HGOTs. Moisture from the wetted tubes allows them to be fused to the HGOTs below. More layers of HGOTs can be moisture-fused to the previous layer after it has been thoroughly dried. Eventually, a three-dimensional interconnected

https://doi.org/10.1021/acsami.3c00546
ACS Appl. Mater. Interfaces 2023, 15, 18940−18950

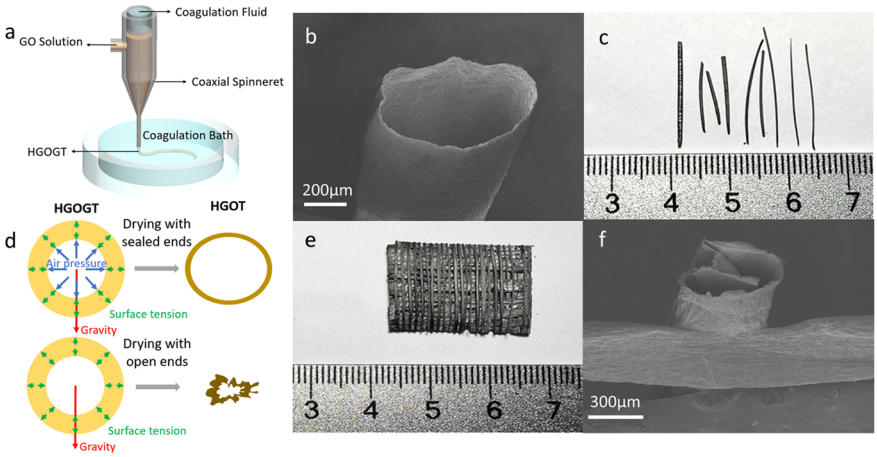

Figure 1. (a) Schematic illustration showing the fabrication of HGOTs by coaxial wet spinning. (b) SEM image of an HrGOT. (c) Digital image of as-prepared HrGOTs. (d) Schematic views of forces acting on the hollow graphene oxide gel tubes during drying. (e) Digital image of an HrGOTA. (f) SEM image of two perpendicularly oriented HrGOTs moisture fused at their outer surfaces.

HGOT assembly can be obtained after the last layer is dried (Figure S1a). HrGOTs and HrGOTAs were obtained from HGOTs and HGOT assemblies, followed by chemical reduction in hydroiodic acid at 80 °C for 24 h and thermal annealing at 1000 °C in a high-purity argon atmosphere for 1 h (Figures S1b,c).

2.3. Fabrication of the HrGOTA-Based Composites. As-purchased MWCNTs were dispersed in a mixture of 50 mL of sulfuric acid and 50 mL of nitric acid and ultrasonicated with an ultrasonic homogenizer for 5 min in a water bath. The dispersed MWCNTs were then refluxed in the acid mixture at 60 °C for 6 h. After removing the acid mixture from the MWCNTs with deionized water and ethanol washing, the acidified MWCNTs were dried, weighed, and added into hot liquid 1-octadecanol so that a mixture of 1-octadecanol and 1 wt % MWCNT is formed. Next, HrGOTAs were immersed in this mixture or pure hot liquid 1-octadecanol, and the immersed HrGOTAs were transferred into a vacuum oven preheated to 80 °C. The vacuum oven was exhausted to 0.1 MPa for 10 min and then vented to facilitate the impregnation of 1-octadecanol or the mixture of MWCNTs and 1-octadecanol into the bores of the HrGOTAs. The vacuuming and venting procedure was repeated three times before the impregnated HrGOTAs were removed from the hot liquid and cooled to room temperature. Finally, the obtained HrGOTA-based composites filled with 1-octadecanol and 1-octadecanol/MWCNT were lightly washed with ethanol to remove the excess 1-octadecanol on their surfaces.

2.4. Material Characterization. The morphology and microstructure of the HrGOTs were characterized by a field-emission scanning electron microscope (SEM) using a Carl Zeiss Supra 55. X-ray diffraction (XRD) patterns were collected with a PAN analytical XRD system at a scanning speed of 4° mm^{-1}. Raman spectroscopy measurements were performed with a LabRAM HR800 Raman microscope using a 532.18 nm green laser light source and 600 grooves mm^{-1} gratings. Fourier transform infrared spectroscopy (FT-IR) was performed on a PerkinElmer Spectrum One FT-IR spectrometer with a 0.5 cm^{-1} resolution. Thermogravimetric analysis (TGA) was performed on a TA Instruments TGA-Q50 under a nitrogen atmosphere from room temperature to 600 °C (Figure S2a). Differential scanning calorimetry (DSC) and modulated DSC were performed on a TA Instruments DSC-Q100 equipped with a refrigerated cooling system from 0 to 100 °C. Modulated DSC was performed to determine the pressure-specific heat capacity of the 1-octadecanol/MWCNT-filled HrGOTA. The spectral absorbance of the HrGOTA-based composites, 1-octadecanol/MWCNT, and 1-octadecanol was characterized using a PerkinElmer Lambda 950 ultraviolet−visible−near-infrared (UV−visible−NIR) spectrometer. The density of the 1-octadecanol/MWCNT-filled HrGOTA sample was measured with an Adam Equipment PW balance.

The thermal conductivity of HrGOTs was measured using an electrical self-heating method. The values were derived from the temperature profile of HrGOTs between two isolated Cu struts in a vacuum chamber with a ZnSe infrared viewport at 10^{-4} Torr. The temperature profile of the HrGOTs was obtained with a FLIR A325sc infrared camera with a microscopic lens (Figures S2b,c). In addition, laser flash analysis (LFA) was performed using a Netzsch LFA 457 Microflash to obtain the thermal diffusivity of the 1-octadecanol/MWCNT-filled HrGOTA composite. The calculation of the thermal conductivity is discussed in detail in the Supporting Information.

2.5. Solar−Thermal Conversion and Storage Efficiency Measurement. The HrGOTA-based PCCs filled with 1-octadecanol and 1-octadecanol/MWCNT were suspended by Kapton tape perpendicularly in front of a 1 cm^2 collimated beam of a Newport 94041A solar simulator in a large vacuum chamber. The irradiance of the collimated beam is 1.0 sun (1000 W m^{-2}). A Fresnel lens with a 26.4 cm diameter and 31.8 cm focal length was used to focus the collimated beam so that an irradiance varying from 1.0 to 4.0 sun could be obtained at specific distances in front of the lens. Using the emissivity determination method described by Li et al.,[5] the infrared emissivity of the HrGOTA-based composites filled with 1-octadecanol and 1-octadecanol/MWCNT was determined. The emissivity of these PCCs was inputted into a FILR A65SC infrared camera which was used to capture infrared videos of the PCCs under solar irradiation through a viewport in the vacuum chamber, which was pumped down to 0.1 Torr. The PCC samples with various layers of interconnected HrGOTs were irradiated. The temperature profiles of these PCC samples were extracted from the infrared videos to study their solar−thermal conversion and storage efficiency. The solar−thermal conversion and storage efficiency of the 1-octadecanol/MWCNT-filled HrGOTA composites with 2 to 5 layers of HrGOTs was studied using their temperature profiles at an irradiance of 4.0 sun.

The solar−thermal conversion and storage efficiency (η) can be calculated by eq 1[40]

$$\eta = \frac{m\Delta H_m}{IS\Delta\tau_m} \approx \frac{m\Delta H_m}{IS(\Delta\tau_f + \Delta\tau_r)} \quad (1)$$

where m, ΔH_m, I, S, $\Delta\tau_m$, $\Delta\tau_f$, and $\Delta\tau_r$ stand for the sample weight under radiation, melting phase change enthalpy, radiation intensity, radiation area, melting phase transition time, freezing phase transition time, and recrystallization time, respectively. No latent heat loss from the PCC samples from convection and conduction is considered, and the PCC samples are diffusing gray bodies, according to Kirchhoff's law of thermal radiation. Therefore

$$\alpha = \varepsilon \quad (2)$$

https://doi.org/10.1021/acsami.3c00546
ACS Appl. Mater. Interfaces 2023, 15, 18940−18950

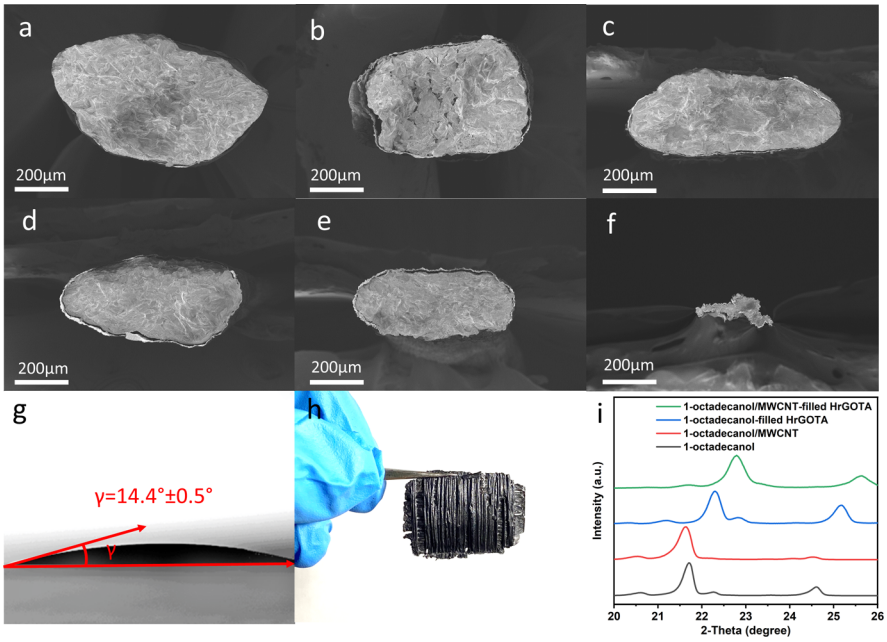

Figure 2. (a–f) Digital images of the 1-octadecanol-filled HrGOT composites prepared from HrGOTs with open-end drying times of 1, 5, 10, 15, 30, and 60 s. (g) Contact angle measurements of liquid 1-octadecanol on an rGO sheet. (h) Digital image of as-prepared 1-octadecanol/MWCNT-filled HrGOTA. (i) Right shift of the XRD patterns of the HrGOTA composites filled with 1-octadecanol and 1-octadecanol/MWCNTs compared to 1-octadecanol and 1-octadecanol/MWCNT.

where ε is the emissivity and α is the absorptivity of the PCC samples. Assuming the difference between the amount of energy absorbed and emitted from the phase change processes is small, and the difference between the phase change temperatures is also small, from

$$\alpha\sigma T_{\alpha}^{4}\Delta\tau_{m} = \varepsilon\sigma T_{\varepsilon}^{4}(\Delta\tau_{f} + \Delta\tau_{r}) \quad (3)$$

where σ is the Stefan–Boltzmann constant, T_{α} is the mean temperature of absorption, and T_{ε} is the mean temperature of emission, it can be deduced that $\Delta\tau_{m} \approx \Delta\tau_{f} + \Delta\tau_{r}$.[41]

3. RESULTS AND DISCUSSION

As a precursor of HrGOTs, HGOTs are first fabricated by coaxial wet spinning (Figures 1a–c). During the fabrication of HGOTs, the draining of the bore coagulation fluid and the subsequent drying of the coagulated hollow graphene oxide gel tube are two crucial steps for ensuring a thin cylindrical wall morphology. Draining the bore coagulation fluid prevents the wrinkling of the HGOT from overcoagulation and allows the gel tubes to be horizontally suspended across a ceramic crucible for drying. During the drying process, the ends of the gel tubes are sealed. The diameter of the gel tubes decreases until the air pressure inside the HGOTs counters the radial compression force caused by the evaporation of the coagulant moisture (Figure 1d). The degree of diameter reduction of the HGOTs depends on the period between the draining of the bore coagulation fluid and the sealing of the two ends of the gel tubes, which can be defined as the open-end drying time. During open-end drying, the radial compression force is exerted onto the gel tubes without resistance. As a result, within 60 s, the diameter of HGOTs decreases linearly with the open-end drying time (Figure S3). To fabricate HrGOTAs, the precursor HGOTs are laid closely in parallel to each other to form a first layer. The density of the HGOTs per layer is around 10 cm^{-1}. For adhering adjacent layers of HGOTs, after draining the bore coagulation fluid, the gel tubes are moisturized by a quick dip into a mixture of water and ethanol and laid perpendicularly to the previous layer. The graphene oxide flakes on the gel tube surface and the portion of the HGOT surface where they are in contact are partially dispersed. The formation of hydrogen bonds between the partially dispersed graphene oxide flakes is therefore facilitated. When the water and ethanol moisture is dried, the hydrogen bonding between two layers of HGOTs persists, forming an interconnected assembly. After the chemical reduction and thermal annealing of the precursor HGOT assembly, HrGOTA is obtained (Figure 1e). The mechanism for adhering two layers of precursor HGOTs is similar to the method of wet fusing;[4] however, with moisture fusing, only the outer surfaces of the HGOTs are moisturized through a quick dipping in an ethanol and water mixture, resulting in the reorganization of graphene oxide (GO) sheets at the surface of the HGOTs. In contrast to the flattened cross sections of wet-fused GFs, HGOTs can maintain their thin cylindrical wall morphology after fusing at the outer surfaces (Figure 1f).

The 1-octadecanol-filled HrGOTs can be obtained by vacuum-impregnating HrGOTs with hot liquid 1-octadecanol (Figure S4). Scanning electron microscopy (SEM) shows that the solidified 1-octadecanol fills the bore of the original HrGOT (Figures 2a–f). When the open-end drying time is short, the cross-sectional area of the HrGOT is relatively smooth (Figure 2a); therefore, almost no gap is observed between 1-octadecanol and HrGOT. By comparing Raman spectra of the 1-octadecanol-filled HrGOT, HrGOT, and 1-octadecanol (Figure S5a) samples, the 1-octadecanol peaks are visible but do not obscure the graphitic G and D peaks of the 1-octadecanol-filled HrGOTs. Therefore, it can be further elaborated that only small amounts of 1-octadecanol adhere to the outer surfaces of the HrGOTs. The high affinity of 1-octadecanol to the HrGOT is shown by a small contact angle of 14.4 ± 0.5° between 1-octadecanol and reduced graphene oxide sheets (rGO) spin-coated onto a glass slide (Figure 2g). Also, using the vacuum impregnation technique, the HrGOTs

https://doi.org/10.1021/acsami.3c00546
ACS Appl. Mater. Interfaces 2023, 15, 18940–18950

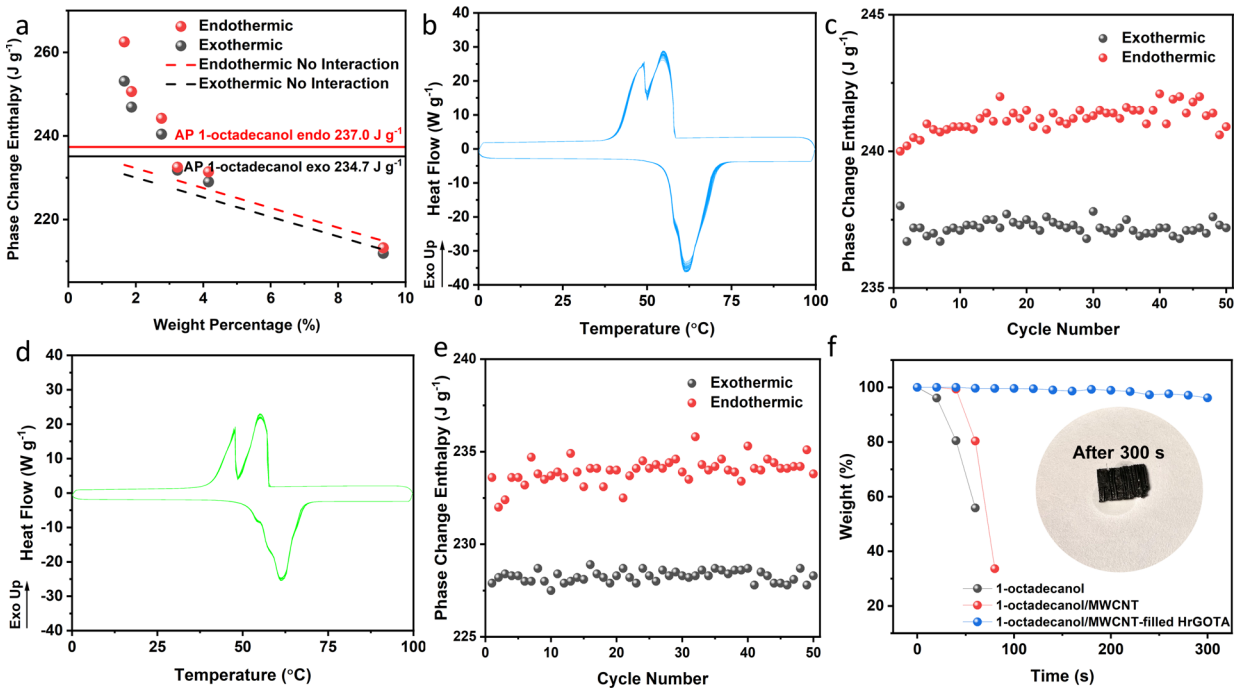

Figure 3. (a) Endothermic and exothermic phase change enthalpies of the 1-octadecanol-filled HrGOTs in relation to their graphene weight percentages. (b) DSC curves of the 1-octadecanol-filled HrGOT under 50 heating−cooling cycles. (c) Endothermic and exothermic phase change enthalpies of the 1-octadecanol-filled HrGOT as a function of heating−cooling cycles. (d) DSC curves of the 1-octadecanol/MWCNT-filled HrGOT under 50 heating−cooling cycles. (e) Endothermic and exothermic phase change enthalpies of the 1-octadecanol/MWCNT-filled HrGOT as a function of heating−cooling cycles. (f) Percentage mass retention of 1-octadecanol, 1-octadecanol/MWCNT, and 1-octadecanol/MWCNT-filled HrGOT under hot plate heating within 300 s.

in an HrGOTA can be filled with a mixture of MWCNTs and 1-octadecanol. As will be discussed in detail, the addition of MWCNTs is beneficial for improving thermal conductivity as well as light absorption in the MWCNT/1-octadecanol-filled HrGOTA PCC (Figure 2h). The majority of the MWCNTs and 1-octadecanol mixture is impregnated into the bores of the HrGOTs, while a small portion adheres to the outer surface of the HrGOTA. The contact angle between the mixture of 1-octadecanol and MWCNT (1-octadecanol/MWCNT) and rGO sheets is measured to be a very small angle of 3.8 ± 0.5°, indicating even better wetting capability of rGO by 1-octadecanol/MWCNT compared to 1-octadecanol (Figure S5b). XRD patterns further confirm the successful impregnation of 1-octadecanol and 1-octadecanol/MWCNT in the HrGOTA. Compared to the XRD patterns of 1-octadecanol and 1-octadecanol/MWCNT, the main peaks of the HrGOTA-based composites' patterns shift to the right by 0.7° and 1.2°, respectively (Figure 2i). According to Debye's law, the shift to the right of these peaks indicates a decrease in the *d* spacing of the 1-octadecanol crystalline lattice, corresponding to a lattice contraction.[42] At the interface of rGO and 1-octadecanol molecules, 1-octadecanol conforms in a herringbone pattern parallel to the inner tube surfaces. In the HrGOTs, 1-octadecanol molecules are crystallized in a head-to-head assembly at an angle of 120°,[43] which is quite different from that in substrate-free crystallization, where the angle is 145°.[44] The smaller angle between adjacent 1-octadecanol molecules results in 1-octadecanol crystallized on a graphitic substrate having a smaller lattice size than free-crystallizing 1-octadecanol. FT-IR patterns of 1-octadecanol/MWCNT and the HrGOTA samples filled by 1-octadecanol and 1-octadecanol/MWCNT show no extra peaks compared to that of 1-octadecanol (Figure S5c), which indicates that no covalent bonds are formed between MWCNTs and 1-octadecanol or between HrGOTs and 1-octadecanol molecules.

For carbon-based PCCs, covalent bonds are generally not desired between the PCM and carbon additives. Their presence leads to latent heat degradation in which the decrease in latent heat percentage of the PCCs becomes greater than their carbon weight percentage. If we define $\Delta H_{endo,1}$ and $\Delta H_{exo,1}$ as the endothermic and exothermic phase change enthalpies of the PCCs, $\Delta H_{endo,0}$ and $\Delta H_{exo,0}$ as the endothermic and exothermic phase change enthalpies of 1-octadecanol, and *f* as the weight percentage of 1-octadecanol in the PCCs, the endothermic and exothermic phase change efficiencies, η_{endo} and η_{exo}, can be defined as follows:[45]

$$\eta_{endo} = \frac{\Delta H_{endo,1}}{\Delta H_{endo,0} f} \tag{4}$$

$$\eta_{exo} = \frac{\Delta H_{exo,1}}{\Delta H_{exo,0} f} \tag{5}$$

Depending on whether the values are smaller than, greater than, or equal to 1, the endothermic and exothermic phase change efficiencies can help identify whether the carbon additives in the PCCs contribute, counteract, or have no effect on the latent heat storage degradation of 1-octadecanol. Interestingly, our DSC studies on the 1-octadecanol-filled HrGOTs show that with 1.66 wt % rGO the η_{endo} and η_{exo} values reach 1.13 and 1.10, respectively. Therefore, we can once more confirm that no covalent bonds exist between the rGO tube and 1-octadecanol. Furthermore, at low rGO weight

https://doi.org/10.1021/acsami.3c00546
ACS Appl. Mater. Interfaces 2023, 15, 18940−18950

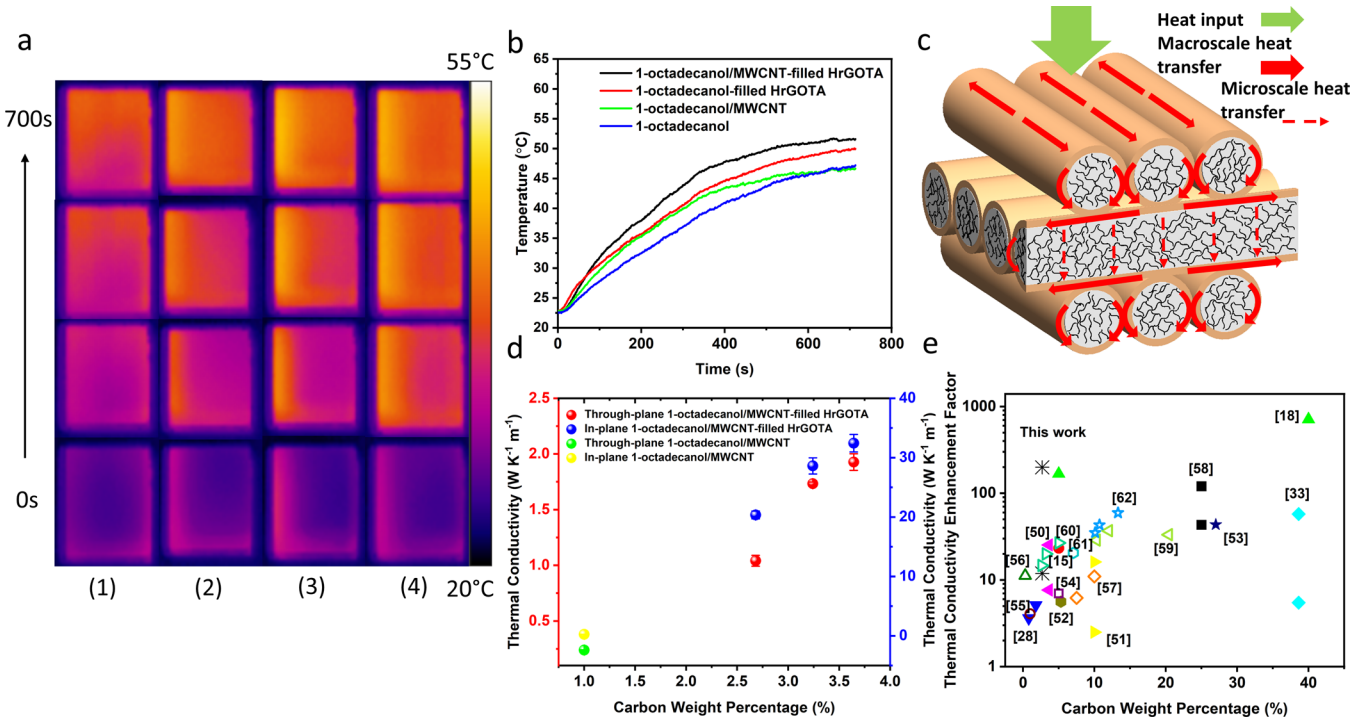

Figure 4. (a) Infrared images of 1-octadecanol (first column), 1-octadecanol/MWCNT (second column), 1-octadecanol filled-HrGOTA (third column), and 1-octadecanol/MWCNT-filled HrGOTA (fourth column) samples heating on a hot plate. (b) Temperature profiles of 1-octadecanol-filled HrGOTA, 1-octadecanol/MWCNT-filled HrGOTA, 1-octadecanol/MWCNT, and 1-octadecanol samples during heating on a hot plate. (c) Schematic illustration of the macroscale and microscale thermally conductive networks in the 1-octadecanol/MWCNT-filled HrGOTA. (d) Through-plane and in-plane thermal conductivities of 1-octadecanol/MWCNT and 1-octadecanol/MWCNT-filled HrGOTA with various carbon weight percentages derived from LFA measurements. (e) Comparison of 1-octadecanol/MWCNT-filled HrGOTA thermal conductivity enhancement with other carbon-based PCCs in recent literature.

percentages, the rGO tube counteracts the latent heat storage degradation of 1-octadecanol (Figure 3a). The SEM cross-sectional images (Figures 2a–c) of the 1-octadecanol-filled HrGOTs show that at low graphene weight percentages, the rGO tube has a smooth inner surface on which 1-octadecanol can crystallize into contracted lattices. It is deduced that the extra potential energy needed to facilitate the increase of latent heat originates from these contracted lattices. As rGO weight percentages increase, the bore cross-sectional area of the rGO tube decreases while the inner surface of the rGO tube becomes increasingly rougher (Figure 2f). These rougher surfaces do not serve well as substrates for 1-octadecanol crystallization. The substrate-free crystallization of 1-octadecanol results in larger, noncontracted lattices, with η_{endo} and η_{exo} values getting closer to 1 (Table S1).

Designing favorable phase change enthalpies and phase transition temperatures is crucial to the real-life energy storage applications of PCCs. The degree of supercooling, which is defined as the difference between the solid-to-liquid and liquid-to-solid phase transition temperatures, is the main indicator of latent heat release quality.[15] The smaller the degree of supercooling, the better the latent heat release quality. The degree of supercooling for the 1-octadecanol-filled HrGOTs with 1.66 wt % graphene reaches a low of 2.46 °C, which is much more favorable than the 7.59 °C of 1-octadecanol. As for the 1-octadecanol/MWCNT-filled HrGOTs, they also maintain favorable phase change enthalpies and phase change transition temperatures. This is confirmed by DSC studies of the HrGOT-based PCCs filled with 1 wt % MWCNT and 1.68 wt % rGO, which show high endothermal and exothermal phase change enthalpies of 234.4 and 233.4 J g^{-1}, respectively. The degree of supercooling reaches a respectable low of 3.24 °C, with η_{endo} and η_{exo} values both being 1.02.

Another aspect of evaluating the favorability of PCCs is their life span. To evaluate the HrGOT-based PCCs life span, DSC thermal cycling experiments are carried out. After heating and cooling between 0 and 100 °C for 50 cycles, both the HrGOT-based PCCs filled by 1-octadecanol and 1-octadecanol/MWCNTs show a high degree of thermal stability, with virtually no change observable for both endothermic and exothermic phase change enthalpies (Figures 3b–e). Another way to study the thermal stability of the PCCs is by directly heating various samples on a hot plate at 80 °C and measuring their mass before and after different heating times. After heating for 300 s, the 1-octadecanol/MWCNT-filled HrGOTA PCC can retain 96.2% of its preheating mass (Figure 3f). After heating for 120 min, the 1-octadecanol/MWCNT-filled HrGOTA PCC can still retain 84.4% of its preheating mass (Figure S6). Compared to 100% mass loss of 1-octadecanol after 75 s and MWCNT/1-octadecano1 after 112 s, the thermal stability of the 1-octadecanol/MWCNT-filled HrGOTA PCC is remarkable and agrees well with the thermal cycling experiments.

From the hot plate heating experiment, it is concluded that the thermal stability of the 1-octadecanol/MWCNT-filled HrGOTA PCCs depends on the structural stabilization effect of the HrGOTA and its thermal conductive property. The heat transfer path in the HrGOTA allows thermal energy to distribute more evenly throughout the PCC; thus, the thermal conductivity of the PCCs determines the potential power of

https://doi.org/10.1021/acsami.3c00546
ACS Appl. Mater. Interfaces 2023, 15, 18940–18950

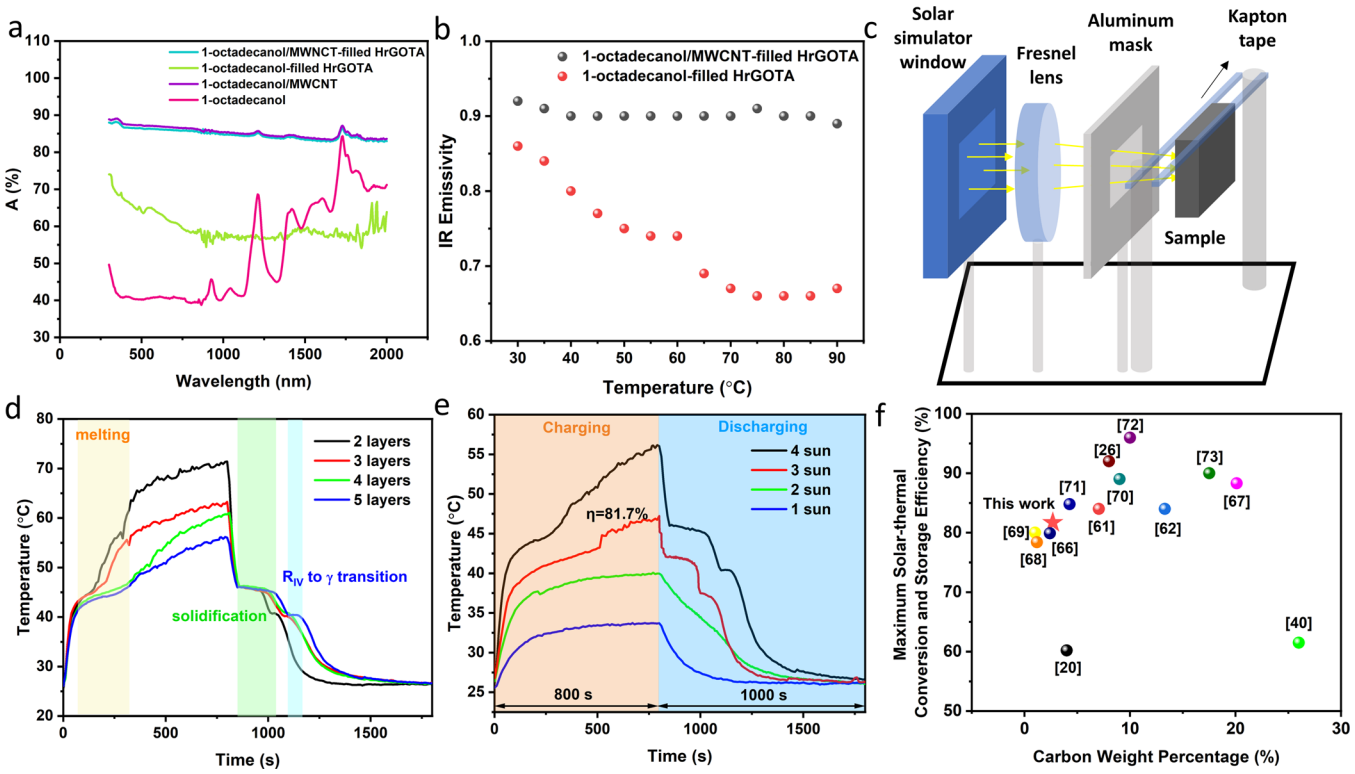

Figure 5. (a) UV−vis−NIR characterization of 1-octadecanol, 1-octadecanol/MWCNT, 1-octadecanol-filled HrGOTA, and 1-octadecanol/MWCNT-filled HrGOTA. (b) Infrared emissivity of 1-octadecanol-filled HrGOTA and 1-octadecanol/MWCNT-filled HrGOTA at various temperatures. (c) Schematic setup of the solar−thermal harvesting experiment of the 1-octadecanol/MWCNT-filled HrGOTA in a solar simulator. (d) Temperature profile of 1-octadecanol/MWCNT-filled HrGOTA with different layers under solar radiation intensity of 4 sun. (e) Temperature profiles of 1-octadecanol/MWCNT-filled HrGOTA with five layers under solar radiation of various intensities. (f) Comparison of the maximum solar−thermal energy conversion and storage efficiency of 1-octadecanol/MWCNT-filled HrGOTA with that of carbon-based PCCs in recent literature.

their thermal energy storage and release. At 0.16 W m^{-1} K^{-1},[46] the thermal conductivity of 1-octadecanol is arguably its main shortcoming. Therefore, it must be composited with a highly thermally conductive material to overcome this shortcoming. The HrGOTs reported in our work serve well for this purpose, exhibiting a thermal conductivity of up to 578.0 W m^{-1} K^{-1}. The high thermal conductivity originates from the improved graphene flake alignment induced by wet spinning shear stress and the absence of phonon scattering defects in the presence of inorganic salts.[1,2] Not only is this a significant improvement to previously reported works on graphene-based hollow tubes,[47−49] but the high thermal conductivity of HrGOTs also serves as the basis for the high thermal conductivity of HrGOTA, which consists of layer-by-layer interconnected HrGOTs.

In HrGOTA-based PCCs, HrGOTA contributes significantly as an excellent thermal conductive backbone, allowing for rapid heat transfer from the energy input area throughout the entire PCC in both the through-plane and in-plane directions. Based on LFA, the through-plane and in-plane thermal conductivities of HrGOTA reach 7.7 and 188.6 W m^{-1} K^{-1}, respectively. An intuitive understanding of the high through-plane thermal conductivity of the HrGOTA-based composites is achieved by heating the HrGOTA-based composites filled with 1-octadecanol and 1-octadecanol/MWCNTs, 1-octadecanol/MWCNT, and 1-octadecanol samples of the same thickness side by side on a hot plate. From the infrared images, it can be found that HrGOTA-based composites have significantly higher through-plane thermal conductivity than 1-octadecanol/MWCNT and 1-octadecanol. The 1-octadecanol/MWCNT-filled HrGOTA sample displays the highest thermal conductivity (Figures 4a,b). The HrGOTA forms an interconnected thermally conductive macroscale network, while the intertangled MWCNTs act as microscale thermally conductive networks in the PCC and supplement the macroscale network (Figure 4c). In-plane and through-plane LFA measurements of the 1-octadecanol/MWCNT-filled HrGOTA samples with 2.68, 3.24, and 3.64 wt % carbon further reveal that through-plane and in-plane thermal conductivities of the 1-octadecanol/MWCNT-filled HrGOTA PCCs increase as their carbon weight percentages increase. At 3.64 wt % carbon, the through-plane and in-plane thermal conductivities reach 1.9 and 31.9 W m^{-1} K^{-1}, respectively (Figures 4d). Despite having a slightly lower through-plane thermal conductivity than recently reported graphene-based PCCs,[15,18,28,33,50−62] the 1-octadecanol/MWCNT-filled HrGOTA PCC achieves excellent in-plane thermal conductivity at a much lower 2.68 wt % carbon (Figure 4e). Lowering the carbon weight percentage is beneficial to the cost control of the PCC's fabrication and allows the PCC to store larger amounts of latent heat with the same total mass. Meanwhile, unlike most graphene-based PCCs, the 1-octadecanol/MWCNT-filled HrGOTA PCC also provides a record-high in-plane thermal conductivity, allowing for better thermal energy distribution throughout the entire PCC when the energy input is uneven on the input surface. This feature is of particular importance for real-life solar−thermal conversion situations.

https://doi.org/10.1021/acsami.3c00546
ACS Appl. Mater. Interfaces 2023, 15, 18940−18950

In solar−thermal conversion applications, a high light absorptivity (A) is highly desired for PCCs. The 1 wt % MWCNTs mixed into 1-octadecanol allows for the resulting 1-octadecanol/MWCNT-filled HrGOTA to obtain a very high absorptivity (A) and very low reflectivity (R) ($A + R = 1$, for nontransparent PCCs) of solar radiation. This is substantiated by UV−vis−NIR spectroscopy of the 1-octadecanol/MWCNT-filled HrGOTA sample (Figure 5a), which shows an absorptivity consistently over 82.9% between the wavelength range of 300 to 2000 nm, including the majority of available energy in solar radiation.[63] Furthermore, the absorption spectrum of the 1-octadecanol/MWCNT-filled HrGOTA closely resembles that of 1-octadecanol/MWCNT. In comparison, the UV−vis−NIR spectrum of the 1-octadecanol-filled HrGOTA samples has an absorptivity of over 54.1%. On the other hand, the absorptivity of 1-octadecanol is only around 40% between 300 and 800 nm and also consistently lower than those of the 1-octadecanol/MWCNT-filled HrGOTA and 1-octadecanol/MWCNT between 800 and 2000 nm. Considering that adding 1 wt % MWCNTs is sufficient in improving the PCC's thermal conductivity and light absorption and that adding more MWCNTs will be detrimental to the latent heat of the PCC, the 1-octadecanol/MWCNT-filled HrGOTA PCCs with higher MWCNT weight percentages are not investigated.

The infrared emissivity of the 1-octadecanol/MWCNT-filled HrGOTA and the 1-octadecanol-filled HrGOTA PCCs is studied using a setup as shown in Figure S7. The emissivity of thin layers of the PCCs pasted to the center of a hot plate is investigated by comparing their infrared images to a piece of carbon black-coated paper with a known wavelength-independent infrared emissivity of 0.95. Using this method, the infrared emissivity of the two PCCs at various measurement temperatures is determined (Figure 5b). The temperature-dependent infrared emissivity is significant for testing the surface temperature evolution of these two PCCs under solar irradiation in a solar simulator chamber (Figure 5c).[64]

The 1-octadecanol/MWCNT-filled HrGOTA PCC samples with 2 to 5 layers are subjected to 4 sun of solar radiation for 800 s in a solar simulator chamber under a 0.1 Torr vacuum. After 800 s, the solar radiation is turned off, and the PCCs are allowed to cool naturally. Several distinct stages are present in the heating and cooling curves of the PCCs, where phase change occurs under simulated solar radiation. In the first stage, the temperature of the PCCs experiences a rapid increase. Then, as the 1-octadecanol in the PCCs undergoes a solid-to-liquid phase transition in a layer-by-layer fashion, a temperature plateau occurs, with that of thicker samples maintained for longer times. After the phase transition of the 1-octadecanol is fully complete, the temperature of the PCCs resumes a slow increase. The thickness determines the maximum temperature on the PCCs' backside. Lower temperatures are measured on PCCs with more layers. After 800 s, the simulated solar radiation is turned off. The temperature of the PCCs rapidly decreases until a temperature plateau occurs again at approximately the same temperature as the previous plateau. In the rGO tubes, 1-octadecanol undergoes a liquid-to-solid phase transition. The liquid-to-solid phase transition plateau stage lasts for a shorter time than the solid-to-liquid phase transition plateau, which is then followed by a transient rapid decrease in temperature. At around 5 °C below the liquid-to-solid phase transition plateau, a temperature plateau occurs once more for an even shorter time. This plateau corresponds with 1-octadecanol's solid-to-solid phase change, where 1-octadecanol transitions from a rotator R_{IV} phase to a monoclinic γ phase.[65]

The exothermic phase change enthalpy of the PCCs corresponds to the total thermal energy released in the liquid-to-solid and rotator-to-crystalline phase change stages. Solar−thermal conversion and storage efficiencies quantify the performance of the PCCs' capability of converting energy from solar radiation into heat and storing it as latent heat, which can be calculated from the heating and cooling curves of the PCCs using eq 1. For the 1-octadecanol/MWCNT-filled HrGOTA PCC samples with 2 to 5 layers, under 4 sun (1 sun = 1000 W m^{-2}) of irradiation, the solar−thermal conversion and storage efficiencies are 40.1%, 37.9%, 45.2%, and 47.8%, respectively (Figure 5d). For the PCC with five layers, the sample was also tested under irradiations of 1, 2, 3, and 4 sun (Figure 5e). The plateau temperature of the five-layered sample linearly correlates with the radiation intensity. Under 1 and 2 sun, the plateau temperatures on the backside of the irradiation do not reach phase change temperature. Under 3 sun, the irradiation is just sufficient to raise the temperature of the entire sample over the phase change temperature. Under this situation, the maximum proportion of the input solar energy is converted into latent heat. As a result, the solar−thermal conversion and storage efficiency reaches 81.7%. This maximum solar−thermal conversion and storage efficiency of the 1-octadecanol/MWCNT-filled HrGOTA PCC is on par with the carbon-based PCCs with the highest reported solar−thermal conversion and storage efficiencies. On the other hand, the carbon weight percentage of the 1-octadecanol/MWCNT-filled HrGOTA PCC is about 20.4 to 66.7% less than other carbon-based PCCs with the highest solar−thermal conversion and storage efficiencies (Figure 5f).[20,26,40,61,62,66−73] 1-Octadecanol and other common PCMs are lighter and cheaper than various forms of carbon additives in carbon-based organic PCCs. Moreover, the higher weight percentage of PCM results in a higher endothermal and exothermal phase change efficiency in the HrGOTA-based PCC (Table S2).[59−62] As a result, the low carbon weight percentage of the HrGOTA-based PCC gives it an extra advantage over its competitors.

4. CONCLUSIONS

In summary, HrGOTs have been fabricated based on coaxial wet spinning and assembled into a 3D HrGOTA structure using moisture fusing. The 1-octadecanol-filled HrGOTA-based PCCs have excellent phase change properties due to the interfacial effect of rGO on the packing of 1-octadecanol lattices. Vacuum impregnated with 1-octadecanol and MWCNT, HrGOTAs not only serve as a structural stabilizing encapsulating framework but also provide a thermally conductive network, allowing HrGOTA-based PCCs to achieve excellent through-plane and in-plane thermal conductivities at low carbon weight percentages. In addition, MWCNTs further improve the PCCs' thermal conductivity while improving the PCCs' visible light absorptivity. The high latent heat, high thermal conductivity, good thermal stability, and high solar radiation absorptivity of the 1-octadecanol/MWCNT-filled HrGOTA PCCs make them excellent materials for solar−thermal energy harvesting and storage. The maximum solar−thermal energy conversion and storage efficiency of the PCCs reaches as high as 81.7%, showing great potential in real-life solar−thermal energy harvesting applications. Moreover, this paper demonstrates the huge potential of

https://doi.org/10.1021/acsami.3c00546
ACS Appl. Mater. Interfaces 2023, 15, 18940−18950

hollow graphene-based tube assemblies in serving as highly thermally conductive and structural stabilizing frameworks in advanced functional composites.

■ ASSOCIATED CONTENT

Supporting Information

The Supporting Information is available free of charge at https://pubs.acs.org/doi/10.1021/acsami.3c00546.

Optical images of HGOTs assembly and HrGOTA; thermal conductivity measurement of HrGOTs and 1-octadecanol/MWCNT-filled HrGOTA; TGA image of 1-octadecanol/MWCNT-filled HrGOTA; bore cross-sectional areas of HrGOTs of various open-end drying times; schematic illustration of 1-octadecanol filled HrGOT fabrication; Raman spectra of 1-octadecanol-filled HrGOT, HrGOT, and 1-octadecanol; contact angle measurement between liquid MWCNT/1-octadecanol and graphene; FT-IR spectra of 1-octadecanol, MWCNT/1-octadecanol, 1-octadecanol-filled HrGOTA, and 1-octadecanol/MWCNT-filled HrGOTA; calculation of 1-octadecanol crystalline parameter change using Bragg's law; percentage mass retention of 1-octadecanol/MWCNT filled-HrGOT under hot plate heating; schematic of infrared emissivity measurement setup; phase change efficiency comparison tables of 1-octadecanol-filled HrGOTs and 1-octadecanol/MWCNT-filled HrGOT; and references (PDF)

■ AUTHOR INFORMATION

Corresponding Author

Jie Lian − *Department of Mechanical, Aerospace, and Nuclear Engineering and Department of Materials Science and Engineering, Rensselaer Polytechnic Institute, Troy, New York 12180, United States;* orcid.org/0000-0002-9060-8831; Email: lianj@rpi.edu

Authors

Mingxin Li − *Department of Mechanical, Aerospace, and Nuclear Engineering, Rensselaer Polytechnic Institute, Troy, New York 12180, United States;* orcid.org/0000-0003-3276-9140

Xuanjie Wang − *Department of Mechanical, Aerospace, and Nuclear Engineering, Rensselaer Polytechnic Institute, Troy, New York 12180, United States*

Lilian Odom − *Department of Mechanical, Aerospace, and Nuclear Engineering, Rensselaer Polytechnic Institute, Troy, New York 12180, United States*

Keith Bryce − *Department of Mechanical, Aerospace, and Nuclear Engineering, Rensselaer Polytechnic Institute, Troy, New York 12180, United States*

Dong Zhao − *Department of Mechanical, Aerospace, and Nuclear Engineering, Rensselaer Polytechnic Institute, Troy, New York 12180, United States*

Junhua Shen − *Department of Materials Science and Engineering, Rensselaer Polytechnic Institute, Troy, New York 12180, United States;* orcid.org/0000-0002-4124-3880

Zongwei Ma − *Department of Chemistry and Chemical Biology, Rensselaer Polytechnic Institute, Troy, New York 12180, United States*

Chulsung Bae − *Department of Chemistry and Chemical Biology, Rensselaer Polytechnic Institute, Troy, New York 12180, United States;* orcid.org/0000-0002-9026-3319

Shankar Narayan − *Department of Mechanical, Aerospace, and Nuclear Engineering, Rensselaer Polytechnic Institute, Troy, New York 12180, United States;* orcid.org/0000-0001-6325-8736

Complete contact information is available at: https://pubs.acs.org/10.1021/acsami.3c00546

Notes

The authors declare no competing financial interest.

■ ACKNOWLEDGMENTS

This work was supported by the US National Science Foundation under Award # DMR 1742806.

■ REFERENCES

(1) Xin, G.; Yao, T.; Sun, H.; Scott, S. M.; Shao, D.; Wang, G.; Lian, J. Highly Thermally Conductive and Mechanically Strong Graphene Fibers. *Science* **2015**, *349* (6252), 1083−1087.

(2) Xin, G.; Zhu, W.; Deng, Y.; Cheng, J.; Zhang, L. T.; Chung, A. J.; De, S.; Lian, J. Microfluidics-Enabled Orientation and Microstructure Control of Macroscopic Graphene Fibres. *Nat. Nanotechnol.* **2019**, *14* (2), 168−175.

(3) Li, M.-F.; Gong, H.; Yan, J.-X.; Wu, Y.-J.; Leng, Y.-C.; Liu, X.-L.; Long, Y.-Z.; Han, W.-P. Fabrication of Thermally Reduced Graphene Micro-Tube and Its Electronic Transport Properties. *Physica E: Low-dimensional Systems and Nanostructures* **2020**, *122*, 114169.

(4) Li, Z.; Xu, Z.; Liu, Y.; Wang, R.; Gao, C. Multifunctional Non-Woven Fabrics of Interfused Graphene Fibres. *Nat. Commun.* **2016**, *7* (1), 13684.

(5) Li, M.; Yang, K.; Zhu, W.; Shen, J.; Rollinson, J.; Hella, M.; Lian, J. Copper-Coated Reduced Graphene Oxide Fiber Mesh-Polymer Composite Films for Electromagnetic Interference Shielding. *ACS Appl. Nano Mater.* **2020**, *3* (6), 5565−5574.

(6) Liu, Z.; Zhang, R.; Yang, K.; Yue, Y.; Wang, F.; Li, K.; Wang, G.; Lian, J.; Xin, G. Highly Thermally Conductive Bimorph Structures for Low-Grade Heat Energy Harvester and Energy-Efficient Actuators. *ACS Appl. Mater. Interfaces* **2022**, *14* (34), 39031−39038.

(7) Li, M.; Lian, J. Microstructure Dictating Performance: Assembly of Graphene-Based Macroscopic Structures. *Acc. Mater. Res.* **2021**, *2* (1), 7−20.

(8) Hu, C.; Zhai, X.; Liu, L.; Zhao, Y.; Jiang, L.; Qu, L. Spontaneous Reduction and Assembly of Graphene Oxide into Three-Dimensional Graphene Network on Arbitrary Conductive Substrates. *Sci. Rep.* **2013**, *3* (1), 1−10.

(9) Fleischer, A. S. *Thermal Energy Storage Using Phase Change Materials: Fundamentals and Applications*; Springer: 2015.

(10) Wu, M.; Wu, S.; Cai, Y.; Wang, R.; Li, T. Form-Stable Phase Change Composites: Preparation, Performance, and Applications for Thermal Energy Conversion, Storage and Management. *Energy Storage Materials* **2021**, *42*, 380−417.

(11) Yuan, K.; Shi, J.; Aftab, W.; Qin, M.; Usman, A.; Zhou, F.; Lv, Y.; Gao, S.; Zou, R. Engineering the Thermal Conductivity of Functional Phase-Change Materials for Heat Energy Conversion, Storage, and Utilization. *Adv. Funct. Mater.* **2020**, *30* (8), 1904228.

(12) Huang, X.; Chen, X.; Li, A.; Atinafu, D.; Gao, H.; Dong, W.; Wang, G. Shape-Stabilized Phase Change Materials Based on Porous Supports for Thermal Energy Storage Applications. *Chem. Eng. J.* **2019**, *356*, 641−661.

(13) Giro-Paloma, J.; Martínez, M.; Cabeza, L. F.; Fernández, A. I. Types, Methods, Techniques, and Applications for Microencapsulated Phase Change Materials (Mpcm): A Review. *Renewable and Sustainable Energy Reviews* **2016**, *53*, 1059−1075.

(14) Liu, C.; Rao, Z.; Zhao, J.; Huo, Y.; Li, Y. Review on Nanoencapsulated Phase Change Materials: Preparation, Characterization and Heat Transfer Enhancement. *Nano Energy* **2015**, *13*, 814−826.

(15) Wu, S.; Li, T.; Wu, M.; Xu, J.; Chao, J.; Hu, Y.; Yan, T.; Li, Q.-Y.; Wang, R. Dual-Functional Aligned and Interconnected Graphite Nanoplatelet Networks for Accelerating Solar Thermal Energy Harvesting and Storage within Phase Change Materials. *ACS Appl. Mater. Interfaces* **2021**, *13* (16), 19200−19210.
(16) Ji, H.; Sellan, D. P.; Pettes, M. T.; Kong, X.; Ji, J.; Shi, L.; Ruoff, R. S. Enhanced Thermal Conductivity of Phase Change Materials with Ultrathin-Graphite Foams for Thermal Energy Storage. *Energy Environ. Sci.* **2014**, *7* (3), 1185−1192.
(17) Qi, G.; Yang, J.; Bao, R.; Xia, D.; Cao, M.; Yang, W.; Yang, M.; Wei, D. Hierarchical Graphene Foam-Based Phase Change Materials with Enhanced Thermal Conductivity and Shape Stability for Efficient Solar-to-Thermal Energy Conversion and Storage. *Nano Research* **2017**, *10* (3), 802−813.
(18) Wu, S.; Li, T.; Tong, Z.; Chao, J.; Zhai, T.; Xu, J.; Yan, T.; Wu, M.; Xu, Z.; Bao, H.; Deng, T.; Wang, R. High-Performance Thermally Conductive Phase Change Composites by Large-Size Oriented Graphite Sheets for Scalable Thermal Energy Harvesting. *Adv. Mater.* **2019**, *31* (49), 1905099.
(19) Xiao, X.; Zhang, P. Morphologies and Thermal Characterization of Paraffin/Carbon Foam Composite Phase Change Material. *Sol. Energy Mater. Sol. Cells* **2013**, *117*, 451−461.
(20) Chen, L.; Zou, R.; Xia, W.; Liu, Z.; Shang, Y.; Zhu, J.; Wang, Y.; Lin, J.; Xia, D.; Cao, A. Electro- and Photodriven Phase Change Composites Based on Wax-Infiltrated Carbon Nanotube Sponges. *ACS Nano* **2012**, *6* (12), 10884−10892.
(21) Zheng, H.; Wang, C.; Liu, Q.; Tian, Z.; Fan, X. Thermal Performance of Copper Foam/Paraffin Composite Phase Change Material. *Energy conversion and management* **2018**, *157*, 372−381.
(22) Yang, Z.; Zhou, L.; Luo, W.; Wan, J.; Dai, J.; Han, X.; Fu, K.; Henderson, D.; Yang, B.; Hu, L. Thermally Conductive, Dielectric Pcm−Boron Nitride Nanosheet Composites for Efficient Electronic System Thermal Management. *Nanoscale* **2016**, *8* (46), 19326−19333.
(23) Chen, X.; Cheng, P.; Tang, Z.; Xu, X.; Gao, H.; Wang, G. Carbon-Based Composite Phase Change Materials for Thermal Energy Storage, Transfer, and Conversion. *Advanced Science* **2021**, *8* (9), 2001274.
(24) Stoller, M. D.; Park, S.; Zhu, Y.; An, J.; Ruoff, R. S. Graphene-Based Ultracapacitors. *Nano Lett.* **2008**, *8* (10), 3498−3502.
(25) Zhao, C.; He, X.; Sheng, N.; Zhu, C. Directional Fiber Framework Wrapped by Graphene Flakes for Supporting Phase Change Material with Fast Thermal Energy Storage Properties. *Journal of Energy Storage* **2023**, *57*, 106304.
(26) Zhang, Y.; Wang, J.; Qiu, J.; Jin, X.; Umair, M. M.; Lu, R.; Zhang, S.; Tang, B. Ag-Graphene/Peg Composite Phase Change Materials for Enhancing Solar-Thermal Energy Conversion and Storage Capacity. *Applied Energy* **2019**, *237*, 83−90.
(27) Wang, W.; Tang, B.; Ju, B.; Gao, Z.; Xiu, J.; Zhang, S. Fe_3o_4-Functionalized Graphene Nanosheet Embedded Phase Change Material Composites: Efficient Magnetic- and Sunlight-Driven Energy Conversion and Storage. *J. Mater. Chem. A* **2017**, *5* (3), 958−968.
(28) Kholmanov, I.; Kim, J.; Ou, E.; Ruoff, R. S.; Shi, L. Continuous Carbon Nanotube−Ultrathin Graphite Hybrid Foams for Increased Thermal Conductivity and Suppressed Subcooling in Composite Phase Change Materials. *ACS Nano* **2015**, *9* (12), 11699−11707.
(29) Zhang, L.; Zhou, K.; Wei, Q.; Ma, L.; Ye, W.; Li, H.; Zhou, B.; Yu, Z.; Lin, C.-T.; Luo, J.; Gan, X. Thermal Conductivity Enhancement of Phase Change Materials with 3d Porous Diamond Foam for Thermal Energy Storage. *Applied Energy* **2019**, *233−234*, 208−219.
(30) Ren, H.; Tang, M.; Guan, B.; Wang, K.; Yang, J.; Wang, F.; Wang, M.; Shan, J.; Chen, Z.; Wei, D.; Peng, H.; Liu, Z. Hierarchical Graphene Foam for Efficient Omnidirectional Solar-Thermal Energy Conversion. *Adv. Mater.* **2017**, *29* (38), 1702590.
(31) Li, Y.; Sun, K.; Kou, Y.; Liu, H.; Wang, L.; Yin, N.; Dong, H.; Shi, Q. One-Step Synthesis of Graphene-Based Composite Phase Change Materials with High Solar-Thermal Conversion Efficiency. *Chem. Eng. J.* **2022**, *429*, 132439.
(32) Ham, H.; Van Khai, T.; Park, N.-H.; So, D. S.; Lee, J.-W.; Na, H. G.; Jung Kwon, Y.; Yeon Cho, H.; Woo Kim, H. Freeze-Drying-Induced Changes in the Properties of Graphene Oxides. *Nanotechnology* **2014**, *25* (23), 235601.
(33) Jiang, Z.; Ouyang, T.; Yang, Y.; Chen, L.; Fan, X.; Chen, Y.; Li, W.; Fei, Y. Thermal Conductivity Enhancement of Phase Change Materials with Form-Stable Carbon Bonded Carbon Fiber Network. *Materials & Design* **2018**, *143*, 177−184.
(34) Zhao, Y.; Jiang, C.; Hu, C.; Dong, Z.; Xue, J.; Meng, Y.; Zheng, N.; Chen, P.; Qu, L. Large-Scale Spinning Assembly of Neat, Morphology-Defined, Graphene-Based Hollow Fibers. *ACS Nano* **2013**, *7* (3), 2406−2412.
(35) Tao, Z.; Chen, X.; Yang, M.; Xu, X.; Sun, Y.; Li, Y.; Wang, J.; Wang, G. Three-Dimensional Rgo@Sponge Framework/Paraffin Wax Composite Shape-Stabilized Phase Change Materials for Solar-Thermal Energy Conversion and Storage. *Sol. Energy Mater. Sol. Cells* **2020**, *215*, 110600.
(36) Zhou, Y.; Liu, X.; Sheng, D.; Lin, C.; Ji, F.; Dong, L.; Xu, S.; Wu, H.; Yang, Y. Polyurethane-Based Solid-Solid Phase Change Materials with in Situ Reduced Graphene Oxide for Light-Thermal Energy Conversion and Storage. *Chem. Eng. J.* **2018**, *338*, 117−125.
(37) Xin, G.; Sun, H.; Hu, T.; Fard, H. R.; Sun, X.; Koratkar, N.; Borca-Tasciuc, T.; Lian, J. Large-Area Freestanding Graphene Paper for Superior Thermal Management. *Adv. Mater.* **2014**, *26* (26), 4521−4526.
(38) Wang, G.; Sun, X.; Lu, F.; Sun, H.; Yu, M.; Jiang, W.; Liu, C.; Lian, J. Flexible Pillared Graphene-Paper Electrodes for High-Performance Electrochemical Supercapacitors. *Small* **2012**, *8* (3), 452−459.
(39) Xu, Z.; Peng, L.; Liu, Y.; Liu, Z.; Sun, H.; Gao, W.; Gao, C. Experimental Guidance to Graphene Macroscopic Wet-Spun Fibers, Continuous Papers, and Ultralightweight Aerogels. *Chem. Mater.* **2017**, *29* (1), 319−330.
(40) Li, G.; Hong, G.; Dong, D.; Song, W.; Zhang, X. Multiresponsive Graphene-Aerogel-Directed Phase-Change Smart Fibers. *Adv. Mater.* **2018**, *30* (30), 1801754.
(41) Balaji, C. Radiative Properties of Non-Black Surfaces. In *Essentials of Radiation Heat Transfer*; Springer: 2021; pp 57−97.
(42) Espeau, P.; Reynolds, P. A.; Dowling, T.; Cookson, D.; White, J. W. X-Ray Diffraction from Layers of N-Alkanes Adsorbed on Graphite. *J. Chem. Soc., Faraday Transactions* **1997**, *93* (17), 3201−3208.
(43) Barnard, R. A.; Matzger, A. J. Functional Group Effects on the Enthalpy of Adsorption for Self-Assembly at the Solution/Graphite Interface. *Langmuir* **2014**, *30* (25), 7388−7394.
(44) Andrushchenko, V.; Pohle, W. Influence of the Hydrophobic Domain on the Self-Assembly and Hydrogen Bonding of Hydroxy-Amphiphiles. *Phys. Chem. Chem. Phys.* **2019**, *21* (21), 11242−11258.
(45) Fu, X.; Lei, Y.; Xiao, Y.; Wang, J.; Zhou, S.; Lei, J. Graft Poly(Ethylene Glycol)-Based Thermosetting Phase Change Materials Networks with Ultrahigh Encapsulation Fraction and Latent Heat Efficiency. *Renewable Energy* **2021**, *179*, 1076−1084.
(46) Al-Ahmed, A.; Sarı, A.; Mazumder, M. A. J.; Hekimoğlu, G.; Al-Sulaiman, F. A.; Inamuddin. Thermal Energy Storage and Thermal Conductivity Properties of Octadecanol-Mwcnt Composite Pcms as Promising Organic Heat Storage Materials. *Sci. Rep.* **2020**, *10* (1), 1−15.
(47) Chakraborty, P.; Datta, P.; Banerjee, D. Composite of Polypyrrole-Graphene Hollow Fibers Mat-a Flexible Thermoelectric Material. In *AIP Conference Proceedings*; AIP Publishing LLC: 2021; Vol. *2327*, p 020009.
(48) Liu, K.; Chen, Z.; Lv, T.; Yao, Y.; Li, N.; Li, H.; Chen, T. A Self-Supported Graphene/Carbon Nanotube Hollow Fiber for Integrated Energy Conversion and Storage. *Nano-Micro Letters* **2020**, *12* (1), 1−11.
(49) Shi, L.; Dai, H.; Ni, Q.; Qi, X.; Liu, W.; He, R.; Chi, Z.; Fu, Y. Controllable Assembly of Continuous Hollow Graphene Fibers with Robust Mechanical Performance and Multifunctionalities. *Nanotechnology* **2022**, *33* (15), 155602.

https://doi.org/10.1021/acsami.3c00546
ACS Appl. Mater. Interfaces 2023, 15, 18940−18950

(50) Min, P.; Liu, J.; Li, X.; An, F.; Liu, P.; Shen, Y.; Koratkar, N.; Yu, Z.-Z. Thermally Conductive Phase Change Composites Featuring Anisotropic Graphene Aerogels for Real-Time and Fast-Charging Solar-Thermal Energy Conversion. *Adv. Funct. Mater.* **2018**, *28* (51), 1805365.
(51) Xin, G.; Sun, H.; Scott, S. M.; Yao, T.; Lu, F.; Shao, D.; Hu, T.; Wang, G.; Ran, G.; Lian, J. Advanced Phase Change Composite by Thermally Annealed Defect-Free Graphene for Thermal Energy Storage. *ACS Appl. Mater. Interfaces* **2014**, *6* (17), 15262−15271.
(52) Yang, J.; Zhang, E.; Li, X.; Zhang, Y.; Qu, J.; Yu, Z.-Z. Cellulose/Graphene Aerogel Supported Phase Change Composites with High Thermal Conductivity and Good Shape Stability for Thermal Energy Storage. *Carbon* **2016**, *98*, 50−57.
(53) Wu, W.; Huang, X.; Li, K.; Yao, R.; Chen, R.; Zou, R. A Functional Form-Stable Phase Change Composite with High Efficiency Electro-to-Thermal Energy Conversion. *Applied Energy* **2017**, *190*, 474−480.
(54) Zhang, Z.; Alva, G.; Gu, M.; Fang, G. Experimental Investigation on N−Octadecane/Polystyrene/Expanded Graphite Composites as Form−Stable Thermal Energy Storage Materials. *Energy* **2018**, *157*, 625−632.
(55) Zhang, N.; Song, Y.; Du, Y.; Yuan, Y.; Xiao, G.; Gui, Y. A Novel Solid-Solid Phase Change Material: Pentaglycerine/Expanded Graphite Composite Pcms. *Adv. Eng. Mater.* **2018**, *20* (10), 1800237.
(56) Amin, M.; Putra, N.; Kosasih, E. A.; Prawiro, E.; Luanto, R. A.; Mahlia, T. M. I. Thermal Properties of Beeswax/Graphene Phase Change Material as Energy Storage for Building Applications. *Applied Thermal Engineering* **2017**, *112*, 273−280.
(57) Bahiraei, F.; Fartaj, A.; Nazri, G.-A. Experimental and Numerical Investigation on the Performance of Carbon-Based Nanoenhanced Phase Change Materials for Thermal Management Applications. *Energy Conversion and Management* **2017**, *153*, 115−128.
(58) Wu, S.; Li, T. X.; Yan, T.; Dai, Y. J.; Wang, R. Z. High Performance Form-Stable Expanded Graphite/Stearic Acid Composite Phase Change Material for Modular Thermal Energy Storage. *Int. J. Heat Mass Transfer* **2016**, *102*, 733−744.
(59) Yang, J.; Li, X.; Han, S.; Zhang, Y.; Min, P.; Koratkar, N.; Yu, Z.-Z. Air-Dried, High-Density Graphene Hybrid Aerogels for Phase Change Composites with Exceptional Thermal Conductivity and Shape Stability. *J. Mater. Chem. A* **2016**, *4* (46), 18067−18074.
(60) Yang, J.; Li, X.; Han, S.; Yang, R.; Min, P.; Yu, Z.-Z. High-Quality Graphene Aerogels for Thermally Conductive Phase Change Composites with Excellent Shape Stability. *J. Mater. Chem. A* **2018**, *6* (14), 5880−5886.
(61) Zhao, H.-Y.; Shu, C.; Min, P.; Li, C.; Deng, W.; Yang, J.; Li, X.; Yu, Z.-Z. Constructing Anisotropic Conical Graphene Aerogels with Concentric Annular Structures for Highly Thermally Conductive Phase Change Composites Towards Efficient Solar−Thermal−Electric Energy Conversion. *J. Mater. Chem. A* **2022**, *10* (42), 22488−22499.
(62) Liu, P.; An, F.; Lu, X.; Li, X.; Min, P.; Shu, C.; Li, W.; Yu, Z.-Z. Highly Thermally Conductive Phase Change Composites with Excellent Solar-Thermal Conversion Efficiency and Satisfactory Shape Stability on the Basis of High-Quality Graphene-Based Aerogels. *Compos. Sci. Technol.* **2021**, *201*, 108492.
(63) Ma, C.; Yan, J.; Huang, Y.; Wang, C.; Yang, G. The Optical Duality of Tellurium Nanoparticles for Broadband Solar Energy Harvesting and Efficient Photothermal Conversion. *Science Advances* **2018**, *4* (8), eaas9894.
(64) Wang, X.; Narayan, S. Thermal Radiative Switching Interface for Energy-Efficient Temperature Control. *Renewable Energy* **2022**, *197*, 574−582.
(65) Gao, X.; Xie, B.; Su, Y.; Fu, D.; Wang, D. Nanoparticle Enlarged Interfacial Effect on Phase Transition of 1-Octadecanol/Silica Composites. *J. Phys. Chem. B* **2015**, *119* (5), 2074−2080.
(66) Tang, X.; Luo, L.; Guo, Y.; Yang, Z.; Zhang, K.; He, R.; Fan, J.; Yang, W. Preparation and Light-to-Heat Conversion Efficiency of Paraffin/Graphene Aerogel Shape-Stable Phase Change Materials. *Fullerenes, Nanotubes and Carbon Nanostructures* **2019**, *27* (5), 375−381.
(67) Yan, D.; Ming, W.; Liu, S.; Yin, G.; Zhang, Y.; Tang, B.; Zhang, S. Polyethylene Glycol (Peg)/Silicon Dioxide Grafted Aminopropyl Group and Carboxylic Multi-Walled Carbon Nanotubes (Sam) Composite as Phase Change Material for Light-to-Heat Energy Conversion and Storage. *Journal of Energy Storage* **2021**, *36*, 102428.
(68) Zhou, Y.; Wang, X.; Liu, X.; Sheng, D.; Ji, F.; Dong, L.; Xu, S.; Wu, H.; Yang, Y. Polyurethane-Based Solid-Solid Phase Change Materials with Halloysite Nanotubes-Hybrid Graphene Aerogels for Efficient Light- and Electro-Thermal Conversion and Storage. *Carbon* **2019**, *142*, 558−566.
(69) Zhang, L.; Li, R.; Tang, B.; Wang, P. Solar-Thermal Conversion and Thermal Energy Storage of Graphene Foam-Based Composites. *Nanoscale* **2016**, *8* (30), 14600−14607.
(70) Yang, J.; Qi, G.-Q.; Liu, Y.; Bao, R.-Y.; Liu, Z.-Y.; Yang, W.; Xie, B.-H.; Yang, M.-B. Hybrid Graphene Aerogels/Phase Change Material Composites: Thermal Conductivity, Shape-Stabilization and Light-to-Thermal Energy Storage. *Carbon* **2016**, *100*, 693−702.
(71) Qian, Y.; Han, N.; Zhang, Z.; Cao, R.; Tan, L.; Li, W.; Zhang, X. Enhanced Thermal-to-Flexible Phase Change Materials Based on Cellulose/Modified Graphene Composites for Thermal Management of Solar Energy. *ACS Appl. Mater. Interfaces* **2019**, *11* (49), 45832−45843.
(72) Sun, K.; Dong, H.; Kou, Y.; Yang, H.; Liu, H.; Li, Y.; Shi, Q. Flexible Graphene Aerogel-Based Phase Change Film for Solar-Thermal Energy Conversion and Storage in Personal Thermal Management Applications. *Chem. Eng. J.* **2021**, *419*, 129637.
(73) Maleki, M.; Ahmadi, P. T.; Mohammadi, H.; Karimian, H.; Ahmadi, R.; Emrooz, H. B. M. Photo-Thermal Conversion Structure by Infiltration of Paraffin in Three Dimensionally Interconnected Porous Polystyrene-Carbon Nanotubes (Ps-Cnt) Polyhipe Foam. *Sol. Energy Mater. Sol. Cells* **2019**, *191*, 266−274.